VTOL-MAV FOR SECURITY AND RESCUE OPERATIONS WITH ENHANCED GEO-POSITIONING CAPABILITIES

R. Mönikes, N. Frietsch, O. Meister, Gert F. Trommer
Institute of Systems Optimization
University of Karlsruhe (TH)
Kaiserstr. 12, 76128 Karlsruhe

ABSTRACT

This paper focuses on the improvement of the navigation solution of a small VTOL-UAV. A smoothing algorithm is investigated which can overcome problems of poor satellite availability. By means of post-processing, it is possible to recover the trajectory during GNSS outages even together with a low-cost MEMS inertial navigation system. Furthermore two methods for the geo-location of objects that are visible in images acquired by the onboard camera are presented. The first one takes into consideration the local height of the earth's surface and is able to handle moving objects. The second algorithm needs no digital elevation model at all and is able to determine the positions of stationary objects with respect to a geo-coordinate system.

1. INTRODUCTION

Over the last years, the interest in unmanned micro aerial vehicles (MAV) has increased constantly. Besides large UAVs that can carry significant payloads, these small aircrafts are important due to their cost efficiency and their ease of deployment. Their possible application area is widespread and ranges from rather basic tasks like the collection of sensor data to more and more complex tasks like surveillance and reconnaissance scenarios. They are especially useful for security and rescue operations for example in case of industrial or natural disasters like earthquakes or fires. For most mentioned applications, the ability to hover is desirable or even essential.

This paper presents an electrically powered four-rotor MAV with a takeoff weight below 1 kg and a diameter of about 90cm (shown in figure 1). It can be used for autonomous missions and manual flight as well. A very important sensor is the on board video camera that acquires necessary information about the observed situations. The image data is stored on board and is optionally transmitted at the same time in flight via a radio down link to the operator at the ground station. The images provide important information about objects and humans in the danger zone and increase the situation awareness of the operator. Especially their exact position with respect to a geographic coordinate system enables an efficient coordination of rescue teams. The operator marks the locations of the objects in the images. Based on the data of the internal camera parameters as well as the position and attitude of the MAV, their positions are autonomously estimated with respect to the desired coordinate system and visualized with the help of geo-referenced maps.

Fig. 1. The MAV with camera used for acquiring image data.

By factoring the position information of subsequent image frames into the considerations, no digital elevation model is required. The accuracy of the resulting position information depends mainly on the accuracy of the navigation solution of the MAV. As the MAV is operated by a human it is possible to fly into regions where no GPS aiding is available, e.g. in the shadow of large building or under trees. It is even possible to fly into buildings as the MAV is very small. Due to cost and weight requirements the MAV can be equipped only with small, lightweight MEMS inertial sensors, which are not able to bridge even short GPS-outages. Therefore smoothing is used to overcome these issues.

The next sections describe the navigation system of the four rotor helicopter and present results of flight tests. The calculation of a precise navigation solution as well as the geo-location of objects, by means of image processing, are also addressed. After a detailed description of the used algorithms the performance of the developed algorithms is illustrated using in-flight UAV sensor and video data.

2. THE NAVIGATION SYSTEM

The navigation system consists of low cost inertial sensors, a GPS receiver, a magnetometer and a

barometric altimeter. It has to operate in two scenarios: In autonomous mode, when the MAV executes autonomously a predefined list of waypoints, it has to provide a full navigation solution comprising position, velocity and attitude. This requires missions that enable continuous GPS availability, e.g. surveillance of facilities. In the manual mode, the MAV is controlled by an operator. A video down link enables the operator to control the MAV without direct line of sight. To make the control of the MAV very easy the attitude is still controlled by the MAV flight controller. The operator has only to care about position and heading. Hence, the navigation system has to provide robust roll and pitch angles, even if GPS is unavailable and the magnetometer is disturbed.

The navigation systems uses a sixteen-state error state space Kalman filter. The state vector $\boldsymbol{x}$ comprises the following states:

Δn, Δe, Δd	Position error with respect to navigation frame.
Δv_n, Δv_e, Δv_d	Velocity error.
$\Delta\phi$, $\Delta\theta$, $\Delta\psi$	Error of roll, pitch and yaw angles.
$\boldsymbol{\omega}_{\text{Bias}}$	Biases of gyroscopes.
$\boldsymbol{a}_{\text{bias}}$	Biases of accelerometers.
b_{alt}	Bias of barometric altimeter.

A simplified system model can be seen in eq. (1) and eq. (2).

$$\dot{\boldsymbol{x}}(t) = \boldsymbol{F}(t)\,\boldsymbol{x}(t) + \boldsymbol{w}(t) \tag{1}$$

(2)

$$\begin{pmatrix} \Delta\dot{v}_n \\ \Delta\dot{v}_e \\ \Delta\dot{v}_d \end{pmatrix} = \begin{pmatrix} 0 & -a_d & a_e \\ a_d & 0 & -a_n \\ -a_e & a_n & 0 \end{pmatrix} \begin{pmatrix} \Delta\phi \\ \Delta\theta \\ \Delta\psi \end{pmatrix} + \boldsymbol{w}$$

With a denoting the specific force and w denoting noise.

The specific force (gravity and accelerations) $\boldsymbol{a}$ couples the velocity errors with the attitude errors. As the gravity, which is part of a_d, is always measured (expect in free fall) roll and pitch angles are observable as long as the vertical velocity is known. Hence, the barometric altimeter stabilizes roll and pitch errors in case GPS is unavailable.

From the third column of the matrix in eq. (2) it follows that the yaw angle is only observable if horizontal accelerations are present. Hence, a magnetometer is necessary to stabilize the yaw angle during hover and stare missions or with GPS unavailable. To make the navigation system robust against disturbances of the magnetometer a simplified measurement model (see eq. (3)) is used. It aids only the yaw angle.

$$\tilde{\boldsymbol{h}}_b - \hat{\boldsymbol{C}}_n^b \boldsymbol{h}_n = \hat{\boldsymbol{C}}_n^b \begin{pmatrix} h_e \\ -h_n \\ 0 \end{pmatrix} \gamma + v \tag{3}$$

with

$\tilde{\boldsymbol{h}}_b$	Normalized measured magnetic field with respect to body coordinates.
$\boldsymbol{h}_n$	True normalized magnetic field with respect to local-level frame.
$\hat{\boldsymbol{C}}_n^b$	Transformation from local-level frame to body coordinates.
v	Noise.

3. SMOOTHING

An advantage of the manual mode is the fact, that the MAV can fly independently of GPS coverage, as the operator controls the speed and the position. Hence it is possible, to fly under trees, bridges, into the shadow of buildings or even into buildings. But for applications in which objects or people shall be geo-located, accurate attitude and position information is still required.

A Rauch-Tung-Striebel smoother (RTS) can overcome these problems.

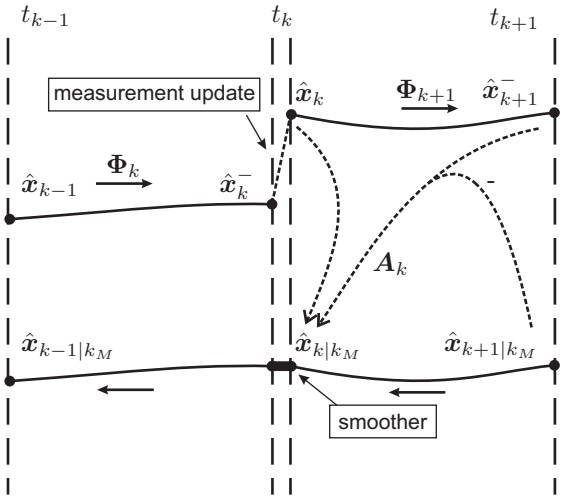

Fig. 2. Forward and reverse run of a RTS smoother.

A RTS smoother may be regarded as an add-on to the Kalman filter. The data processing can be divided in two steps. In the first step the RTS smoother acts as an Kalman filter, but every time the system state vector changes, it and its variance-covariance matrix is logged into a file. If the system state changes in the propagation step of the KF, the state vector and the propagation matrix are logged, too. But if the state changes due to a measurement update, no measurement data is logged, because it is not needed by the algorithm.

In the second step, only the logged data is used by the algorithm. It is processed backward in time. The algorithm recursively estimates a new system state, by means of maximum likelihood.

In comparison to the KF, the RTS smoother calculates the most likely estimation of the state vector of a linear dynamic system on the condition that past, current and future measurements are known. It is only applicable in post processing, but promises improved accuracy, especially during GPS outages.

Fig. 2 illustrates how the data is used. The upper part shows the forward run and the lower part the reverse run and the involved variables. The meanings of the variables are as follows:

t_k	Time of measurement update or system state update, if the system state is updated between measurements.
$\hat{\boldsymbol{x}}_k^-$	Estimation of the system state at t_k on the condition that the measurements of t_1, t_2, ..., t_{k-1} are known.
$\hat{\boldsymbol{x}}_k$	Estimation of the system state at t_k on the condition that the measurements of t_1, t_2, ..., t_k are known.
$\hat{\boldsymbol{x}}_{k\|k_M}$	Estimation of the system state at t_k on the condition that the measurements of t_1, t_2, ..., t_{k_M} are known. $k_M \geq k$
$\boldsymbol{\Phi}_k$	Propagation matrix: $\hat{\boldsymbol{x}}_k^- = \Phi_k\, \hat{\boldsymbol{x}}_{k-1}$.
$\boldsymbol{A}_k$	Weighting matrix.

Between two GPS measurements the KF predicts the system state $\hat{\boldsymbol{x}}_k^-$, by means of inertial navigation. When a new GPS measurement becomes available, the KF calculates a new corrected prediction $\hat{\boldsymbol{x}}_k$. But the longer the time between the measurements is, the greater the errors will become. Hence the KF trajectory contains great discontinuities. The smoother has the ability to level these discontinuities, by means of a new weighting of the previously calculated system states $\hat{\boldsymbol{x}}_k^-$, $\hat{\boldsymbol{x}}_k$ and $\hat{\boldsymbol{x}}_{k|k_M}$. The final trajectory therefore is smooth and contains no discontinuities.

The full smoother equations are:

$$\boldsymbol{A}_k = \boldsymbol{P}_k \boldsymbol{\Phi}_k^T \left(\boldsymbol{P}_{k+1}^-\right)^{-1} \tag{4}$$

$$\hat{\boldsymbol{x}}_{k|k_M} = \hat{\boldsymbol{x}}_k + \boldsymbol{A}_k \left(\hat{\boldsymbol{x}}_{k+1|k_M} - \hat{\boldsymbol{x}}_{k+1}^-\right) \tag{5}$$

were $\boldsymbol{P}$ denotes the covariance matrix of $\vec{x}$. $\boldsymbol{P}_{k|k_M}$ can be calculated as follows, but is not needed for the algorithm:

$$\boldsymbol{P}_{k|k_M} = \boldsymbol{P}_k + \boldsymbol{A}_k \left(\boldsymbol{P}_{k+1|k_M} - \boldsymbol{P}_{k+1}^-\right) \boldsymbol{A}_k^T \tag{6}$$

If a smoother is used to bridge GPS outages, sufficient measurement data before and after the outage has to be logged. Processing of the smoother equations requires lot of processing-time and the storage of a large amount of intermediate data. This can not be done by the small micro-controller of a drone. Hence all the measurement data is stored and processed after the flight. In future it will be possible to transmit the measurement data in real-time to the operator. Then it is possible to calculate the smoothed navigation solution with only short delays. On a modern PC post-processing of 10 minutes of flight data requires only 30s.

4. FLIGHT TESTS

To test the capabilities of the smoother, a flight test was performed. To obtain a good reference solution the flight took place with full GPS coverage all the time and the MAV operated in autonomous waypoint mode. GPS outages have been simulated afterwards during post-processing.

In the first test the data was post-processed with a Kalman filter and a smoother with no GPS outages.

One problem occurring in real-time conditions is the determination of the absolute height. The barometric altimeter provides a very accurate relative height information but its bias is initially unknown.

The GPS height is not very reliable, as the error may become very large (several tens of meters) in situations with few satellites and bad DOP values (dilution of precession).

Fig. 3 shows the height estimation of the Kalman filter and the smoother. The GPS-height and the relative barometric height is also shown. The flight data includes take-off and landing, which took place at the same location. It can be seen that GPS-height starts with a large height error, as the height at the beginning differs by approx. 20m from the height at the end. The barometric height shows only little differences between take-off and landing.

The Kalman filter height overshoots at the beginning and approaches then to the real height. The overshoot is because of the fact that the Kalman filter has first to estimate the biases of the inertial sensors. The figure also shows that the smoother optimally merges the height measurements. It adopts the relative height information of the barometric sensor and places it a the weighted mean GPS height.

The next test was done with simulated GPS-outages. During one test only one GPS measurement was provided every 20 seconds for a longer period. The results of the horizontal position estimation can be seen in Fig. 5. The figure shows the reference position from the calculation with no outages. The Kalman filter and the smoothed solution are also shown. Four waypoints are also included into the figure. The GPS measurements are indicated by small circles.

It can be seen that the inertial solution of the Kalman filter immediately drifts far off as soon as GPS measurements stay away. The reason for that is that the low-cost inertial sensors are suitable for control tasks but not for stand alone inertial navigation. Nevertheless it is possible to recover the

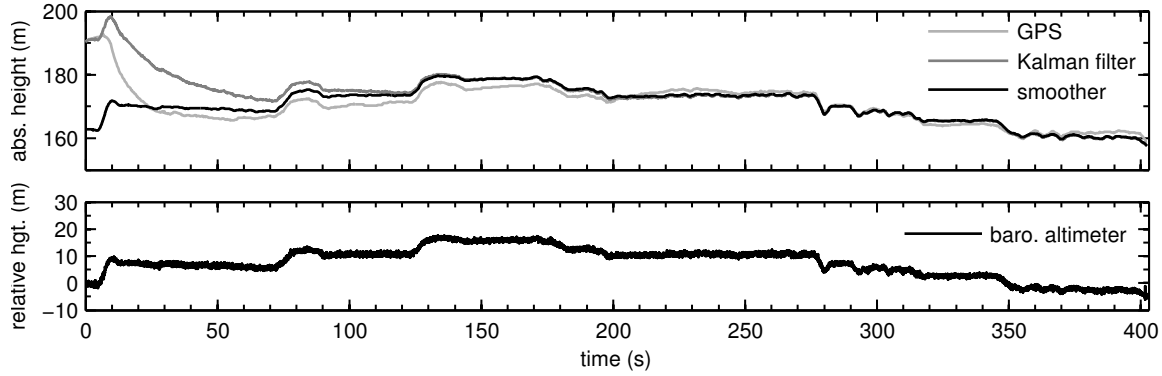

Fig. 3. Comparison of height estimation. The smoother optimally merges the GPS-height with the barometric heigth.

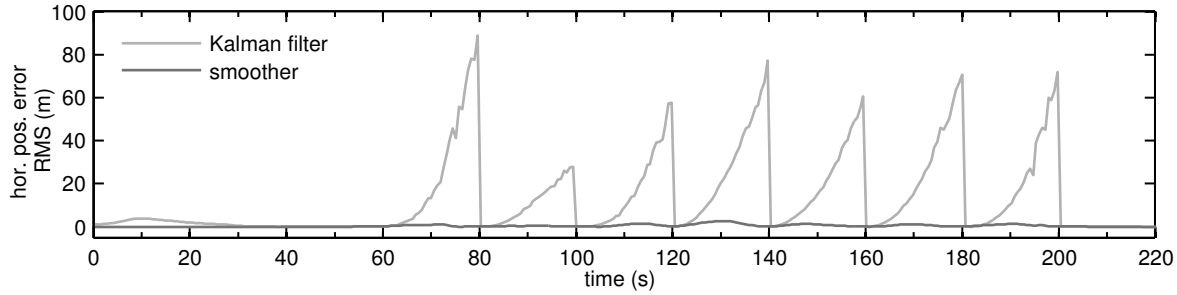

Fig. 4. Comparison horizontal position errors in presence of GPS outages.

flight path with the smoother very well. Only small deviations from the reference position remain. A more quantitative plot can be seen in Fig. 4. It shows the horizontal position error with respect to the smoothed solution with no GPS-outages. It can be seen that the position error of the Kalman filter grows very fast until a new GPS-measurement arrives. Then the error is reset, but starts to grow again. The error of the smother reaches its maximum between two GPS-measurements, but is by far smaller than that of the Kalman filter.

In another test the same data was processed with one large GPS-outage lasting 60s. The position solution can be seen in Fig. 6. Again the position of the Kalman filter is immediately far of. The maximum error (not shown in the figure) is over 300 meters. The error of the smoothed solution is again quite smaller but some artifacts remain in the flight path. The maximum of the position error is 23 meters.

5. GEO-LOCATION OF OBJECTS IN IMAGE DATA

In this section, the geo-location of objects for example humans, cars or buildings in images that are acquired by the onboard camera during the flight is described. The positions of the objects of interest can be either retrieved by suitable detection and tracking algorithms [**?**] [**?**] or the operator marks the locations of the objects in the images. In both cases, the positions of the objects are given in pixel coordinates. However, in a catastrophe scenario for example, where a human operator coordinates the rescue teams, the knowledge of the geo-coordinates of the relevant objects is very important.

The geo-location of an object i in an image with known 2D pixel coordinates $(x_i,\, y_i)^T$ is the determination of its coordinates with respect to a desired 3D geo-coordinate system. This implies the knowledge of the position and orientation of the camera in the 3D world as well as the internal parameters describing the optical path inside the camera.

The position and attitude of the used MAV are determined by the onboard navigation system. Its position $\vec{x}^{\,e}_{MAV}$ [1] is given in ECEF-coordinates (see Fig. 7), that can be transformed into latitude lat_{MAV}, longitude $long_{MAV}$ and altitude above sea level h_{MAV}. The attitude of the MAV is given by the three Euler angles $\phi_{nb}, \theta_{nb}, \psi_{nb}$ or the direction cosine matrix $\mathbf{C}_{nb}$, respectively, that describe the rotation between the body fixed coordinate system and the so called navigation coordinate system shown in Fig. 7 pointing in a northward, eastward and downward direction.

As the camera is fixed on the chassis under the center of mass of the helicopter, the simplification is justified that the center of the so called camera coordinate system, located in the projection center of the camera and the center of the body coordinate system coincide. Their coordinate transformation is

[1] In the following the superscript character specifies the coordinate system with respect to which the variable is given.

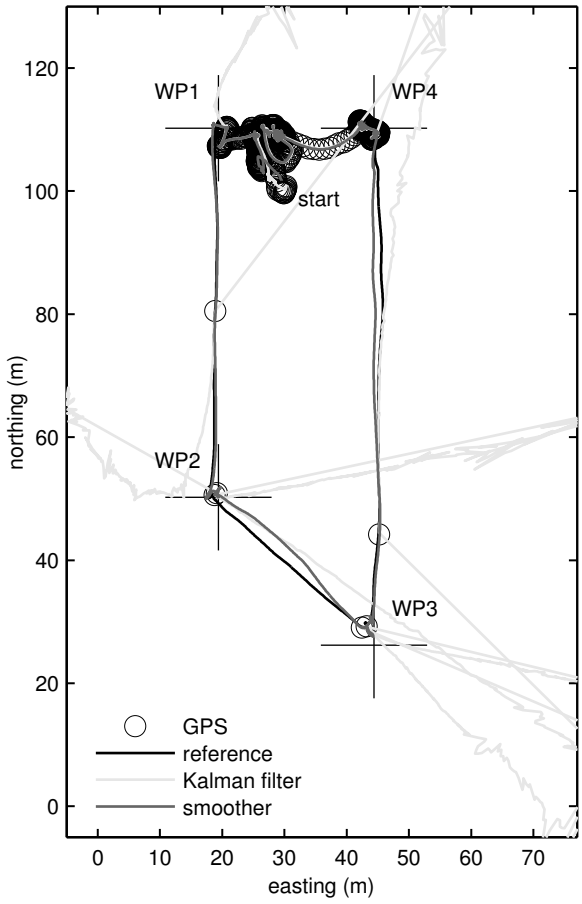

Fig. 5. Results

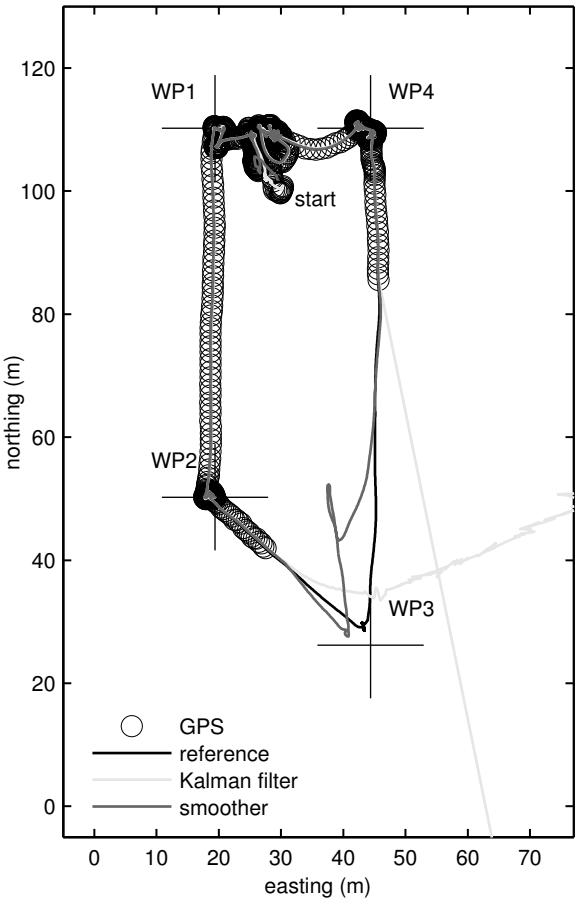

Fig. 6. Results

described by the three Euler angles $\phi_{bc}, \theta_{bc}, \psi_{bc}$ or the direction cosine matrix $\mathbf{C}_{bc}$, respectively. The error of this simplification is much smaller than the position error of the MAV. Furthermore the intrinsic camera parameters have to be estimated. As the radial distortion introduced by the wide angle lens was compensated before the detection process, a simple pinhole camera model is sufficient. The position $\vec{x}_i^C$ of the object i with respect to the camera coordinate system is therefore given with the help of the so called camera calibration matrix $\mathbf{K}$ [1] by a transformation

$$\vec{x}_i^c = \begin{pmatrix} x_i^c \\ y_i^c \\ z_i^c \end{pmatrix} = \mathbf{K} \cdot \begin{pmatrix} x_i \\ y_i \\ 1 \end{pmatrix} = \mathbf{K} \cdot \vec{x}_{i,hom}. \tag{7}$$

This position vector is the same as the direction vector from the origin of the camera coordinate system towards the position of the object in the real world. It can be transformed into coordinates with respect to the navigation coordinate system by the following equation:

$$\vec{x}_i^n = \mathbf{C}_{nb} \cdot \mathbf{C}_{bc} \cdot \vec{x}_i^c = \mathbf{C}_{nb} \cdot \mathbf{C}_{bc} \cdot \mathbf{K} \cdot \vec{x}_{i,hom}. \tag{8}$$

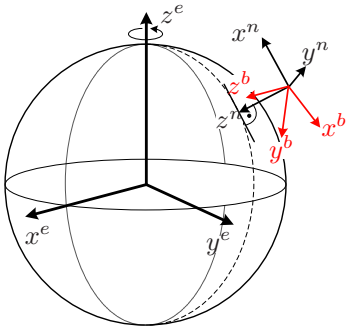

Fig. 7. The definitions of the ECEF-, the navigation- and the body-coordinate system.

The first method for geo-location bases on the assumption, that the earth's surface can be locally approximated by the tangent plane E of the earth with the altitude above sea level h_{Earth}

$$E: \quad z_{Earth}^n = (h_{MAV} - h_{Earth}). \tag{9}$$

The position $\vec{x}_o^n$ of the considered object in the real world with respect to the navigation coordinate system is the intersection of the line through origin defined by the direction vector $\vec{x}_i^n$, see eq. (7), with

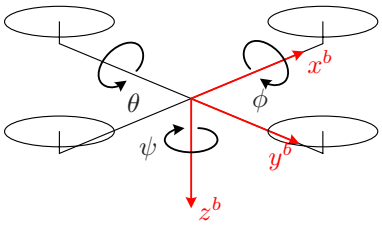

Fig. 8. The definitions of the body-coordinate system and the three Euler angles.

the plane E

$$\vec{x}_o^n = (h_{MAV} - h_{Earth}) \cdot \begin{pmatrix} x_i^n / z_i^n \\ y_i^n / z_i^n \\ 1 \end{pmatrix}. \quad (10)$$

After having transformed the data into the appropriate coordinate system, the results can be suitable visualized by plotting it onto a georeferenced map. The used maps of the city Karlsruhe (Germany) are given with respect to the Gauß-Krüger coordinate system. In Fig. 9, the results of an automatic detection and tracking of a moving car are shown exemplarily as well as the according geo-located positions of the car in Fig. 10. This method may be even improved in the future by taking into account DTED information.

Fig. 9. Two frames of a stabilized image sequence with the detected and tracked object that is marked with white boxes.

Fig. 10. Geo-located trajectory of the tracked object in Fig. 9, the mean position of the used MAV is marked with a white cross.

The second method for geo-location needs no knowledge about the local elevation profile of the earth's surface as the position information of subsequent frames is taken into consideration. Therefore the time index k that refers to the takings of the images is used in the following. The considered objects need to be stationary. The point defined by the vector $\vec{x}_{i,k}^n$ (see eq. (8)) can be transformed into ECEF-coordinates $\vec{x}_{i,k}^e$ with the knowledge of $\vec{x}_{MAV,k}^e$. The straight line g_k from the origin of the body coordinate system towards the position of the object in the real world at time k is now determined by these two points $\vec{x}_{MAV,k}^e$ and $\vec{x}_{i,k}^e$. These lines are calculated for all epochs k where information about the position of the considered object is available. The pairwise intersection point of two of them or the point that is closest to both lines, is an estimation for the position of the object in ECEF-coordinates.
The auxiliary variable $\vec{l}_k^e$ is defined as follows

$$\vec{l}_k^e = \vec{x}_{i,k}^e - \vec{x}_{MAV,k}^e \quad (11)$$

as well as the variables $s_{k1,k2}$ and $t_{k1,k2}$ for two different times k_1 and $k2$:

$$s_{k1,k2} = \frac{(\vec{x}_{i,k2}^e - \vec{x}_{i,k1}^e) \cdot (\vec{l}_{k2}^e \times (\vec{l}_{k1}^e \times \vec{l}_{k2}^e))}{(\vec{l}_{k1}^e \times \vec{l}_{k2}^e)^2} \quad (12)$$

$$t_{k1,k2} = \frac{(\vec{x}_{i,k2}^e - \vec{x}_{i,k1}^e) \cdot (\vec{l}_{k1}^e \times (\vec{l}_{k1}^e \times \vec{l}_{k2}^e))}{(\vec{l}_{k1}^e \times \vec{l}_{k2}^e)^2}. \quad (13)$$

The estimated position of the object in ECEF-coordinates when taking into consideration the data at time $k1$ and $k2$ is given by

$$\vec{x}_{o,estim.}^e = 0.5 \cdot (\vec{x}_{i,k1}^e + \vec{x}_{i,k2}^e + s_{k1,k2} \cdot \vec{l}_{k1}^e + t_{k1,k2} \cdot \vec{l}_{k2}^e). \quad (14)$$

In Fig. 11, two frames of a processed image sequence are shown. The marked corner of the building is geo-located and the result is shown in Fig. 12. The translational displacement of the MAV during the processed takings of the images is big enough to ensure a good geometric configuration of the straight lines.

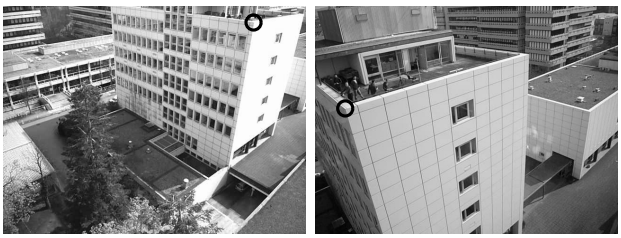

Fig. 11. Positions of corner of house in frame 21 and 271 of an image sequence marked by black circle.

6. CONCLUSION

In this paper two algorithms for geo-locating image data have been presented. The first one works well

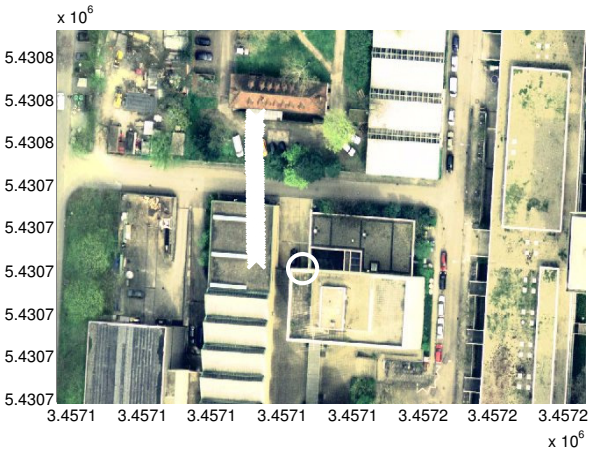

Fig. 12. Geo-located corner of house from Fig. 11; the estimated position is marked with a white circle, the positions of the MAV are marked with white crosses.

for moving objects taking into consideration information about the local height profile. The second algorithm is able to geo-locate stationary objects without any additional knowledge of the local surface profile of the earth. The performances of both algorithms are restricted by the precision of the navigation solution of the MAV. To increase the accuracy of the navigation system, a smoother was developed. Measurement results have shown that the smoother is able to bridge short outages, and to improve the fusion of the GPS height with the barometric height. These techniques enable a good geo-location of image data. Even though post-processing is required, the coordinates of objects can be provided after a few minutes. The accuracy of the geo-located positions enables e.g. the coordination and guidance of rescue teams.

REFERENCES

[1] Hartley R., Zisserman A., *Multiple View Geometry, Second Edition*. Cambridge: Cambridge University Press, 2003.
[2] R. E. Kalman, “A new approach to linear filtering and prediction problems,” *ASME Journal of Basic Engineering*, vol. 82, no. D, pp. 35 – 45, 1960.
[3] H. E. Rauch, F. Tung, and C. T. Striebel, “Maximum likelyhood estimates of linear dynamic systems,” *AIAA Journal*, vol. 3, no. 8, pp. 1445 – 1450, 1965.
[4] S. Nassar, E.-H. Shin, X. Niu, and N. El-Sheimy, “Accurate INS/GPS positioning with different inertial systems using various algorithms for bridging GPS outages,” *ION GNSS 18th Internationl Technical Meeting of the Satellite Division, 13-16 September 2005, Long Beach, CA*, pp. 1401 – 1410, 2005.
[5] E.-H. Shin and N. El-Sheimy, “Backward smoothing for pipeline surveying applications,” *ION-NTM 2005*, pp. 921 – 927, 2005.
[6] E.-H. Shin and D. N. El-Sheimy, “Optimizing smoothing computation for near real-time GPS measurement gap filling in INS/GPS systems,” *ION-GPS 2002*, pp. 1434 – 1441, 2002.
[7] C. Hide and T. Moore, “GPS and low cost INS integration for positioning in the urban environment,” *ION GNSS 18th Internationl Technical Meeting of the Satellite Division, 13-16 September 2005, Long Beach, CA*, pp. 1007–1015, 2005.
[8] S. Kennedy, J. Hamilton, and H. Martell, “Architecture and system performance of SPAN-NovAtel’s GPS/INS solution,” pp. 266–274, 2006.